ACCURATE MATCHING AND RECONSTRUCTION OF LINE FEATURES FROM ULTRA HIGH RESOLUTION STEREO AERIAL IMAGES

A. O. Ok [a] *, J. D. Wegner [b], C. Heipke [b], F. Rottensteiner [b], U. Soergel [b], V. Toprak [a]

[a] Dept. of Geodetic and Geographic Information Tech., Middle East Technical University, 06531 Ankara, Turkey
- (oozgun, toprak)@metu.edu.tr
[b] Institute of Photogrammetry and Geoinformation, University of Hannover, 30167 Hannover, Germany
- (wegner, heipke, rottensteiner, soergel)@ipi.uni-hannover.de

Commission III, WG III/4

KEY WORDS: Line Matching, Line Reconstruction, Height Estimation, Projective Geometry, Stereo Aerial Images

ABSTRACT:

In this study, a new reconstruction approach is proposed for the line segments that are nearly-aligned ($\leq 10º$) with the epipolar line. The method manipulates the redundancy inherent in line pair-relations to generate artificial 3D point entities and utilize those entities during the estimation process to improve the height values of the reconstructed line segments. The best point entities for the reconstruction are selected based on a newly proposed weight function. To test the performance of the proposed approach, we selected three test patches over a built up area of the city of Vaihingen–Germany. Based on the results, the proposed approach produced highly promising reconstruction results for the line segments that are nearly-aligned with the epipolar line.

1. INTRODUCTION & MOTIVATION

The matching and reconstruction of line segments in ultra high resolution stereo aerial images is a very challenging task due to various reasons; substantial change in viewpoints, inconsistency of line endpoint locations, the limitations of the line geometric constraints imposed, lack of rich textures in line local neighbourhood, repetitive patterns etc. Up to now, a significant number of research papers have been devoted to stereo line matching (ex: Schmid and Zisserman, 1997; Baillard and Dissard, 2000; Scholze et. al., 2000; Zhang and Baltsavias, 2000; Suveg and Vosselman, 2004; Herbert et. al., 2005; Wang et. al., 2009; Ok et. al., 2010a, b); however, the ambiguity of line matching is an issue that remains unsolved. Moreover, in addition to the problems of matching, the reconstruction of the matched line segments under stereo geometry is also a challenging issue and the final accuracy of the reconstructed line segments is still limited to certain imaging conditions.

So far, the general attempt to solve line matching problems in stereo geometry has relied on various descriptors specialized for one to one line matching in which the relations between the line features are not effectively taken into account. However, the integration of the line to line relations during matching not only exposes new constraints to improve the performance of matching (Ok et. al., 2010a, b), but also provides new opportunities for better estimation of the height values of the line endpoints during the reconstruction stage. In a recent work, we presented a novel approach for the pair-wise matching of line segments from stereo aerial images (Ok et. al., 2010a), and later we further developed and extended the approach to deal with repetitive linear patterns problem (Ok et. al., 2010b). In this paper, our motivation and contribution is mainly on the height estimation of the matched segments. Although the method of direct construction gives satisfactory reconstruction results for the lines that are not aligned with the epipolar line, a dramatic decrease in terms of height accuracy for the lines that are nearly or exactly aligned ($\leq 10º$) with the epipolar line is inevitable (Fig. 1). This is due to the reason that if the angles of lines in image space get closer to the epipolar direction, the two projection planes generated from line segments become similar and in the worst case (exact alignment) they turn out to be the same plane. For those cases, the direct construction of 3D lines from the intersection of planes is highly problematic in terms of

final height accuracy and may be even some cases the intersection (or the reconstruction) may not be possible. Therefore, in this paper, we propose a new reconstruction method which also relies on line to line relations developed in the pair-wise approach. The main idea is to manipulate the redundancy inherent in pair-relations to generate artificial 3D point entities ($\mathbf{X}_i$) from available pair matches and utilize those points during the estimation process to improve the height estimation of the matched segments. However, since we do not exactly know whether the two lines in a pair really intersect on the Earth surface or not, before the estimation process, we select the proper point entities by means of a new weight function which is composed of mainly three terms computed in a pair-wise manner; Euclidean distance, epipolar constraint and intersection angle in image space. For each problematic matching case ($\leq 10º$), we automatically select the appropriate artificial 3D point entities and integrate each selected entity during the estimation process along with the projection planes of the problematic line segments. Thus, at the end of this joint estimation, we have a possibility to reconstruct those problematic line segments with promising final accuracies.
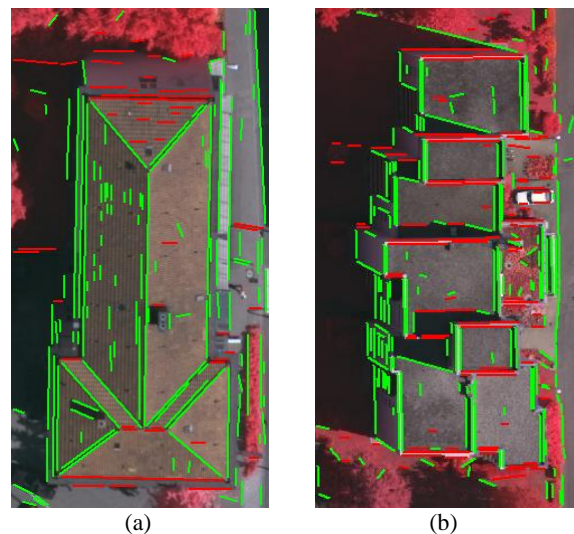

Fig. 1 Line segments extracted from test images. The red ones indicate the lines that are aligned ($\leq 10º$) with the epipolar line.

2. MATCHING OF LINE SEGMENTS

For the matching of line features, we recently proposed a new relational approach in which the line correspondences between the stereo aerial images are established using a pair-wise manner. In this paper, we only briefly summarize the matching algorithm and refer the reader to the references for further details (Ok et. al., 2010a, b). The algorithm consists of three fundamental steps; (i) 2D line extraction, (ii) stereo matching of the extracted lines with a pair-wise relation approach, and (iii) iterative pair-based post-processing.

In the first step, in order to maximize the performance of the line detection, existing multispectral information in aerial images was fully utilized throughout the steps of pre-processing and edge detection. To accurately describe the straight edge segments, a principal component analysis technique was adapted and the extracted segments were converted to their line counterparts using orthogonal regression. In addition, during the raster to vector conversion, we also allowed the curved structures to be approximated by their piecewise linear representations. In the second step, to establish the pair-wise line correspondences between the stereo images, a new pair-wise stereo line matching approach was utilized. The developed approach initially generates reference line pairs in the base image and collects all potential matching candidate pairs from the search image with the aid of a-priori known image to image geometry. Next, the number of matching candidate pairs of each line pair in the base image are significantly reduced after imposing a weighted pair-wise matching similarity score computed over a total of eight pair-wise constraints (an epipolar, three geometric, two photometric, a correlation and a spatiogram constraint). In the last step, an iterative pair-based post-processing algorithm was utilized. For each line in the base image, the best corresponding line in the search image was assigned after an iterative final disambiguation process in which the matching inconsistencies were further eliminated using nearest/next distance ratios and a final similarity voting scheme.

3. RECONSTRUCTION OF LINE SEGMENTS

It is well-known that the reconstruction of straight lines which are nearly parallel to the epipolar line is almost impossible within a stereo image pair or a single image strip (Zhang, 2005). For that reason, Zhang (2005) proposed an alternative way which relies on free-form line structures generated from multiple line segments. However, the major difficulty with the free-form structures is that the problematic line(s) must have an edge connection with the other neighbouring lines; however, this is rarely the case for most of the line segments. Here, we present a new approach which also relies on line to line relations developed in the pair-wise approach. Thus, we have a possibility to reconstruct those problematic line segments without having such an edge connectivity assumption.

The reconstruction process starts with a test which determines the angle difference (0 – 90º) between the line segments and the related epipolar line. Based on our experiences, the line segments that have angle differences of less than 10 degrees are highly susceptible to produce inaccurate reconstruction results. Therefore, during the test, we label the lines as not-aligned if the angle difference is computed to be larger than 10 degrees. The reconstruction of all those matched line segments are performed by intersecting the projection planes (Fig. 2), $\mathbf{A}^1(l_1)$ and $\mathbf{A}^2(l_2)$, with the method of direct construction as introduced in Heuel and Förstner (2001) and Heuel (2001).
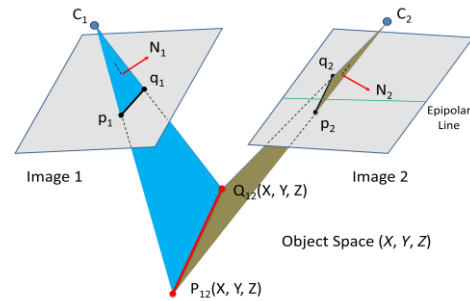

Fig. 2 The reconstruction of the line segments that are not aligned with the epipolar line.
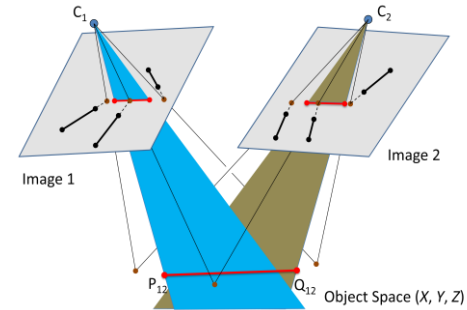

Fig. 3 The reconstruction of the line segments that are nearly-aligned with the epipolar line.

The underlying approach for the reconstruction of line segments that are nearly-aligned ($\leq 10º$) with the epipolar line is to manipulate the redundancy (Ok et. al., 2010b) inherent in pair-relations to generate artificial 3D point entities ($\mathbf{X}_i$) and utilize those points during the estimation process. By this way, the neighbouring line segments that have a pair-connection with the problematic segment contribute to the height estimation (Fig. 3). However, the reconstruction cannot be performed in a single framework, since all 2D intersection points generated lie exactly on the problematic line segments; thus also belong to the projection planes. Therefore, each artificial 3D point entity ($\mathbf{X}_i$) must be generated beforehand, and the final estimation should be jointly performed along with the related projection planes ($\mathbf{A}_i$). In this section, we follow the similar representation of the homogeneous uncertain vectors given in Heuel and Förstner (2001).

3.1 The Generation of Uncertain Artificial 3D Point Entities:

Formally the uncertain homogeneous vectors are denoted as ($\mathbf{x}$, $\mathbf{\Sigma}_{xx}$), where $\mathbf{\Sigma}_{xx}$ is the covariance matrix of the homogeneous vector $\mathbf{x}$. A 2D uncertain line ($\mathbf{l}$, $\mathbf{\Sigma}_{ll}$) in image space can be generated by joining the end-points of the line segment, ($\mathbf{x}$, $\mathbf{\Sigma}_{xx}$) and ($\mathbf{y}$, $\mathbf{\Sigma}_{yy}$):

$$(\mathbf{l}, \mathbf{\Sigma}_{ll}) = \left(\mathbf{x} \times \mathbf{y}, S(\mathbf{y})\,\mathbf{\Sigma}_{xx}\,S(\mathbf{y})^T + S(\mathbf{x})\,\mathbf{\Sigma}_{yy}\,S(\mathbf{x})^T\right) \quad (1)$$

where skew-symmetric matrix $S(\mathbf{x})$ and $S(\mathbf{y})$ are the matrix representation of the points $\mathbf{x}$ and $\mathbf{y}$, respectively. Similar to Eq. 1, the intersection point $\mathbf{x}$ of two lines $\mathbf{l}$ and $\mathbf{m}$ can be computed as

$$(\mathbf{x}, \mathbf{\Sigma}_{xx}) = \left(\mathbf{l} \times \mathbf{m}, S(\mathbf{l})\,\mathbf{\Sigma}_{mm}\,S(\mathbf{l})^T + S(\mathbf{m})\,\mathbf{\Sigma}_{ll}\,S(\mathbf{m})^T\right) \quad (2)$$

with the related skew-symmetric matrices, $S(\mathbf{l})$ and $S(\mathbf{m})$. In our case, initially, the covariance matrices of each line endpoints are
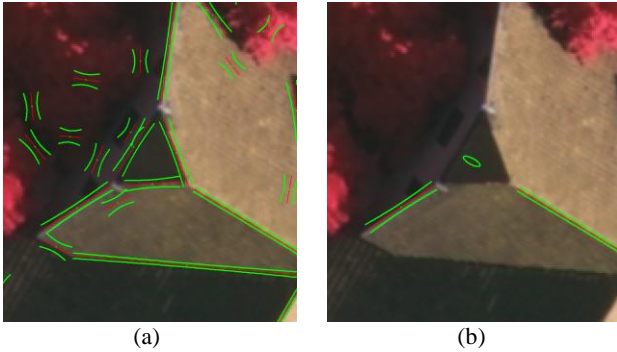
Fig. 4 (a) Confidence regions of extracted line segments, (b) an example of the generated artificial intersection point and its elliptical confidence region. Entities and confidence regions are shown in red and green colors, respectively. Confidence regions are 15 times exaggerated for visualization.

computed from edges that form the line segment, the details can be found in (Madsen and Christensen, 1995). Next, the lines and their uncertainties are computed from those endpoints using Eq. 1 (Fig 4a). Thereafter, for each problematic segment, the neighbouring line segments that have a pair-connection with the problematic segment is collected (from the available pair-wise matches) and their intersection points are computed using Eq. 2. Fig. 4b illustrates an example of a generated artificial intersection point with its elliptical confidence region.

The estimation of the artificial 3D point entities ($\mathbf{X}_i$) from 2D correspondences cannot be performed using direct construction; since the projecting rays emerge from 2D points rarely intersect in object space. Therefore, we estimated the 3D points using the iterative linear estimation model Gauss-Helmert with constraints. The details of the Gauss-Helmert model can be found in Förstner (2005) and McGlone et. al. (2004). In our case, we have 6 observations for each case (two homogeneous 3 vectors for image points $\mathbf{x}_i$) and 4 unknowns for the homogeneous coordinates of each 3D point entity. Thus, referring to the Gauss-Helmert model, we have the vector $\boldsymbol{l}$ of the observations and the vector $\boldsymbol{u}$ of the unknown parameters:

$$l_{6\times 1} = \begin{bmatrix} \mathbf{x}_{i1} \\ \mathbf{x}_{j2} \end{bmatrix} \qquad u_{4\times 1} = \mathbf{X}_{ij} \qquad (3)$$

With the aid of the reduced skew-symmetric matrices $S^{[r]}(.)$, there are 2 independent constraints $\boldsymbol{g}$ for each observed image point $\mathbf{x}$ and the unknown parameters ($\mathbf{X}_{ij}$). In addition, we have a single length constraint h on the unknown parameters. Thus, the relations of the Gauss-Helmert model for the estimation of the 3D point entities can be written as:

$$g(l, u)_{4\times 1} = \begin{bmatrix} S^{[r]}(\mathbf{x}_{i1})P_1\mathbf{X}_{ij} \\ S^{[r]}(\mathbf{x}_{j2})P_2\mathbf{X}_{ij} \end{bmatrix} = \mathbf{0}$$

$$h(u) = {X_{ij}}^T X_{ij} - 1 = 0 \qquad (4)$$

where P_1 and P_2 are the 3x4 projection matrices for points on images 1 and 2, respectively. The initial approximate values of $\mathbf{X}_{ij}$ for the iterative solution can be obtained from the SVD solution (Heuel and Förstner, 2001), and once the estimation is completed, the covariance matrices of the estimated 3D point entities can be computed from the inverted normal equation matrix.

3.2 The Joint Estimation of the 3D Line Segments

For the estimation procedure, we parameterize the 3D lines in Plücker representation $\boldsymbol{L}^T = \left(\boldsymbol{L}_h^T, \boldsymbol{L}_0^T\right) = (L_1, L_2, L_3; L_4, L_5, L_6)$ and utilize an iterative linear Gauss-Markoff model with constraints. The algebraic expressions of the form $\mathbf{g}_i(\beta; \gamma_i) = \mathbf{0}$ with respect to all possible observation and unknown entities are developed and explicitly given in Förstner et. al. (2000) and Heuel and Förstner (2001). In our case, we are searching for an unknown line $\mathbf{M}$ which primarily must lie in two planes; thus, $\mathbf{g}_1(\mathbf{M}; \mathbf{A}_i) = \Pi^T(\mathbf{A}_i)\mathbf{M} = \mathbf{0}$ where Π is the homogeneous matrix representation of planes $\mathbf{A}_i$. The projection planes $\mathbf{A}_i$ for each line $\mathbf{l}_i$ and the related uncertainties can be determined using the projection matrices P_j of the images:

$$\mathbf{A}_{ij} = P_j^T \mathbf{l}_{ij}$$

$$\Sigma_{\mathbf{A}_{ij}\mathbf{A}_{ij}} = P_j^T \Sigma_{\mathbf{l}_{ij}\mathbf{l}_{ij}} P_j + \left(I_4 \otimes \mathbf{l}_{ij}\right)\Sigma_{P_jP_j}\left(I_4 \otimes \mathbf{l}_{ij}^T\right) \qquad (5)$$

where, I_n represents n x n unit matrix and $\otimes$ denotes the Kronecker product. The uncertainty of each line is derived from Eq. 1 and for this study; we assumed that the projection matrices are free of error. In addition to the projection planes, the unknown line must also satisfy the generated artificial 3D point entities ($\mathbf{X}_i$) generated from the neighbouring line segments, $\mathbf{g}_2(\mathbf{M}; \mathbf{X}_i) = \overline{\Pi}^T(\mathbf{X}_i)\mathbf{M} = \mathbf{0}$, where $\overline{\Pi}$ is the homogeneous matrix form of points $\mathbf{X}_i$. However, since we do not exactly know whether the two lines in a pair really intersect on the Earth surface or not, before the estimation process we compute weights for each 3D point entity generated. The weights utilized depend on three measures computed in a pair-wise manner; minimum 2D Euclidean distance (d_{ij}) between two lines (l_i and l_j), the minimum angle (θ_{ij}) enclosed by line segments l_i and l_j, and the minimum orthogonal distance (d_{ij}^e) between the intersection points and related epipolar lines (l_{epi}). In principle, reliability of a point increases if the distances (both d_{ij} and d_{ij}^e) computed are relatively short and decreases if the intersection angle is quite narrow (ex. $< 10°$). Therefore, we designed the new cumulative weight function (W_{ij}) as:

$$W_{ij} = t_{ij} \cdot e^{-\left(\frac{\sigma_2 d_{ij} + \sigma_1 d_{ij}^e}{2\sigma_1\sigma_2}\right)}$$

$$t_{ij} = \begin{cases} 0 & \text{if } \theta_{ij} \leq 10° \\ 1 & \text{if } \theta_{ij} > 10° \end{cases} \qquad (6)$$

where the parameter σ_1 and σ_2 controls the weighting for metrics d_{ij} and d_{ij}^e, respectively. Fig. 5 shows the weighting curves separately computed for each measure.
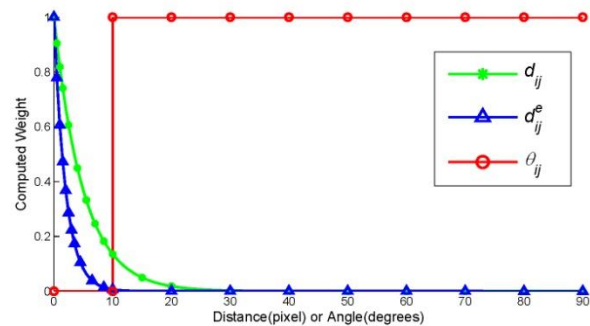

Fig. 5 Independent weight curves for each measure. The control parameters (σ_1 and σ_2) are (5 and 2), respectively.

For each nearly-aligned matching case ($\leq 10^{\circ}$), the existing 3D point entities ($\mathbf{X}_i$) are collected and their weights (W_{ij}) are automatically determined using Eq. (6). However, it is not logical to integrate all observed point entities directly to the estimation process, since some of those points may be generated from wrong matches. Therefore, first, we eliminate all point entities that have weights less than a pre-defined threshold ($T_w \leq 0.01$). Thereafter, among the remaining point entities, only the points that have the highest weights are integrated to the estimation process along with the observed projection planes. However, the selection approach for the best point entities is not trivial and must be carefully handled. Fig. 6 demonstrates a case in which a matching line (l_e) is aligned with the epipolar line. Assume that l_e is paired with three neighbouring lines (l_1, l_2, and l_3) after matching. We estimate the related 3D point entities ($\mathbf{X}_1$, $\mathbf{X}_2$, and $\mathbf{X}_3$) from each corresponding intersection point (p_1, p_2, and p_3) using the Eqs. 1-4. and compute the related weights (W_1, W_2 and W_3) for each entity from Eq. 6. However, it is clear that the entities ($\mathbf{X}_2$ and $\mathbf{X}_3$) will get higher weights than entity $\mathbf{X}_1$, since the computed minimum 2D Euclidean distance (d_{ij}) measure for $\mathbf{X}_1$ is significantly larger than the other distances. Thus, for this case, the 3D line will be estimated from the entities ($\mathbf{X}_2$ and $\mathbf{X}_3$) along with the projection planes ($\mathbf{A}_{e1}$ and $\mathbf{A}_{e2}$). However, since those entities are very close to each other and are located just one side (right) of the lines (l_{e1} and l_{e2}) the final position of the line segments in object space is highly sensitive to the small deviations between the entities $\mathbf{X}_2$ and $\mathbf{X}_3$, which may significantly reduce the final accuracy of the 3D line estimated. To solve this problem, we propose a region based weighting of points (Fig 6 c-d) in which the highest weighted points are calculated for each region separately. We utilize two split points ($l/3$, $2l/3$) to divide the direction dominated by each line into three classes, left (R_L) – center (R_C) – right (R_R). Next, best weights are computed for each region separately. Thus, we guarantee that the point entity ($\mathbf{X}_1$) generated by the intersection points (p_{11} and p_{12}) contributes to the final estimation.

For the estimation process, we form the point-line and plane-line incidence relations in 3D space and perform an iterative
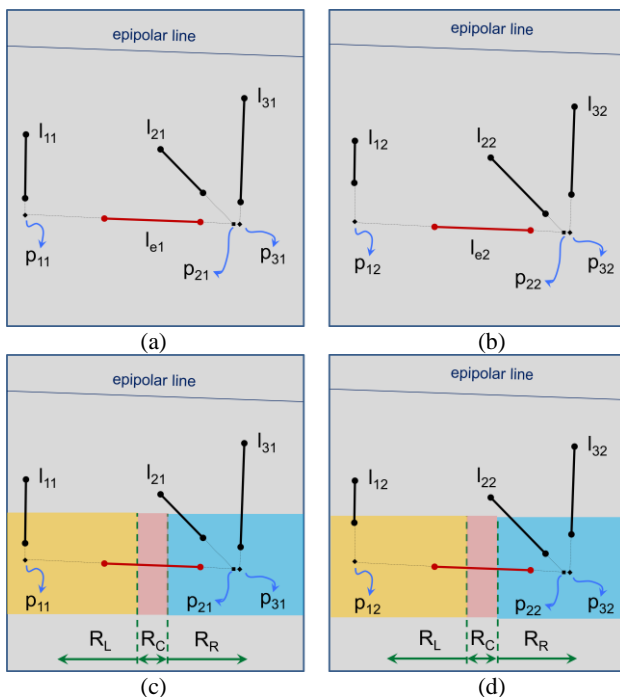
linear Gauss-Markoff model with constraints. For each case, we have 6 unknowns and 2 constraints (Plucker and length) for each 3D line ($\mathbf{L}_i$). In addition to the two projection planes, the final observation number depends on the number of point entities $\mathbf{X}_i$ available for each region. Once again, the required initial values can be taken from the SVD solution and the covariance matrices of the estimated 3D line entities can be computed from the inverted normal equation matrix of the Gauss-Markoff model.

4. TEST SITES AND RESULTS

Three test patches (Fig. 7) are chosen from the city of Vaihingen, Germany (Cramer and Haala, 2009). For those test
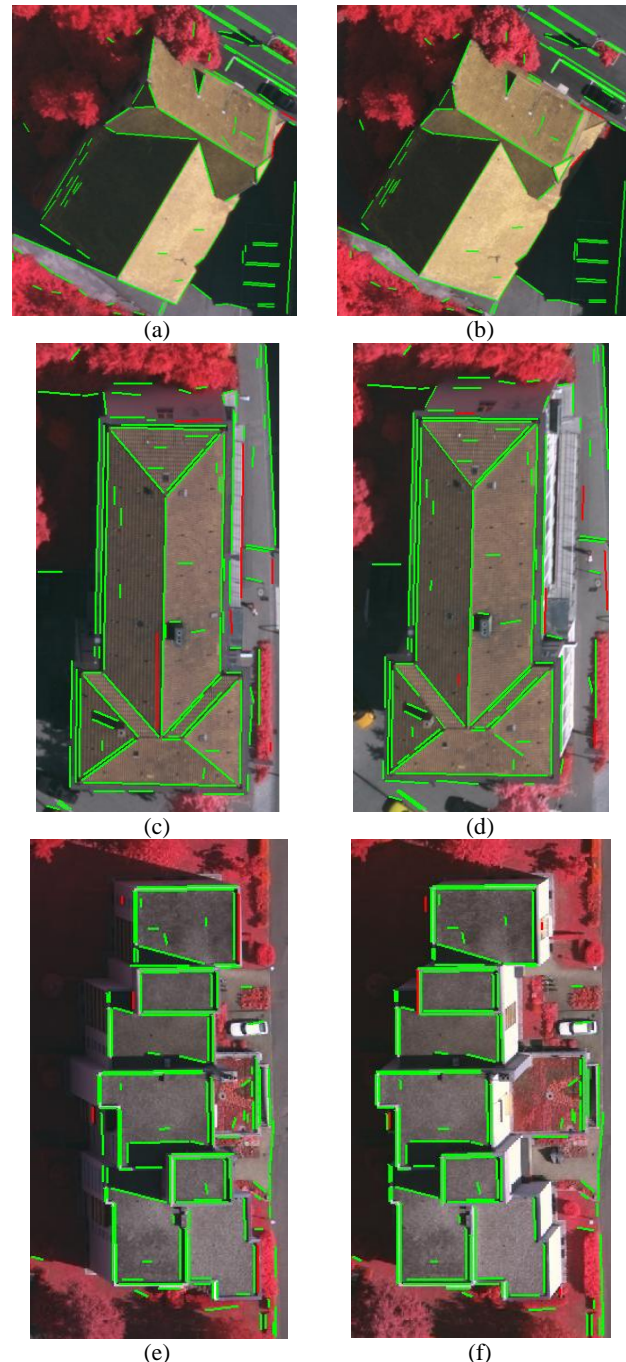

(a)

(b)

(c)

(d)

(e)

(f)

Fig. 7. Test patches. Left (a-c-e) and right (b-d-f) stereo images. Correct and false matches are shown in green and red colors, respectively.

(a)

(b)

(c)

(d)

Fig. 6 Left (a-c) and right (b-d) stereo images. The directional regions utilized during the selection of the best weighted point entities.

Table 1. The matching performance of the pair-wise approach.

Patch ID	Number of			Level of		
	Correct	False	Missed	Corr.	Comp.	Quality
1	101	3	2	97%	98%	95%
2	94	6	5	94%	95%	90%
3	111	5	14	96%	89%	85%

patches, stereo images were acquired by the DMC digital camera with 800 m above the ground level which corresponds to final ground sampling distances (GSD) of approximately 8 cm. During the experiments, for all test patches, we applied a 50 m (≈ 162 pixels) search range difference (between the min. and max. heights) along the epipolar lines. In order to assess the performance of the matching, the number of correct and false line matches was assessed manually. We also investigated the number of matches missed by the pair-wise matching approach; thus, the results in terms of completeness, correctness and quality levels (Rutzinger et. al., 2009) for each test patch are also provided (Table 1). Based on the results computed, for all test patches, consistent correctness levels (> 94%) are achieved. Similarly, the computed completeness levels for all patches are comparable; however, the highest number of matches (= 14) is missed for the third image pair. This is due to the nature of the pair-wise approach; most of those missed matches are located on the ground level and could not be paired correctly with other ground level line segments. It is also clear that there is a significant correlation between the computed quality levels and the number of line segments that are found to be aligned with

the epipolar line. The highest matching quality (95%) is achieved for the first patch in which the number of nearly-aligned line segments is relatively less observed compared to the other patches. On the other hand, the lowest matching quality (85%) is observed for the third image patch in which approximately half of the extracted line segments are nearly-aligned with the epipolar line (Fig. 1).

Despite the successful matching performances, the method of direct construction produced dramatic reconstruction problems for the lines that are nearly-aligned with the epipolar line (Fig 8 a-d-g). It is clear from those figures that the reconstruction results of the line segments that are nearly-aligned with the epipolar line are extremely defective and irrelevant. On the other hand, our approach successfully recovered most of those problematic cases (Fig. 8 b-e-h). Although we believe that the level of improvement is visually apparent, we also evaluated the accuracy of the reconstructed line segments by comparing them to LIDAR data. The LIDAR data of the test site were captured with a Leica ALS50 system with an accuracy of 3.4 cm (Haala, 2009). In order to compare the reconstructed lines, we automatically extracted 3D planes from the point cloud in the vicinity of each line (Fig. 8 c-f-i). Depending on the type of the line, this plane reconstruction process resulted in one plane if the line corresponded to a step edge and in two planes if the line corresponded to the intersection of two planes. Thereafter, we determined the line's average orthogonal distance from its neighbouring planes and used these distances to compute the
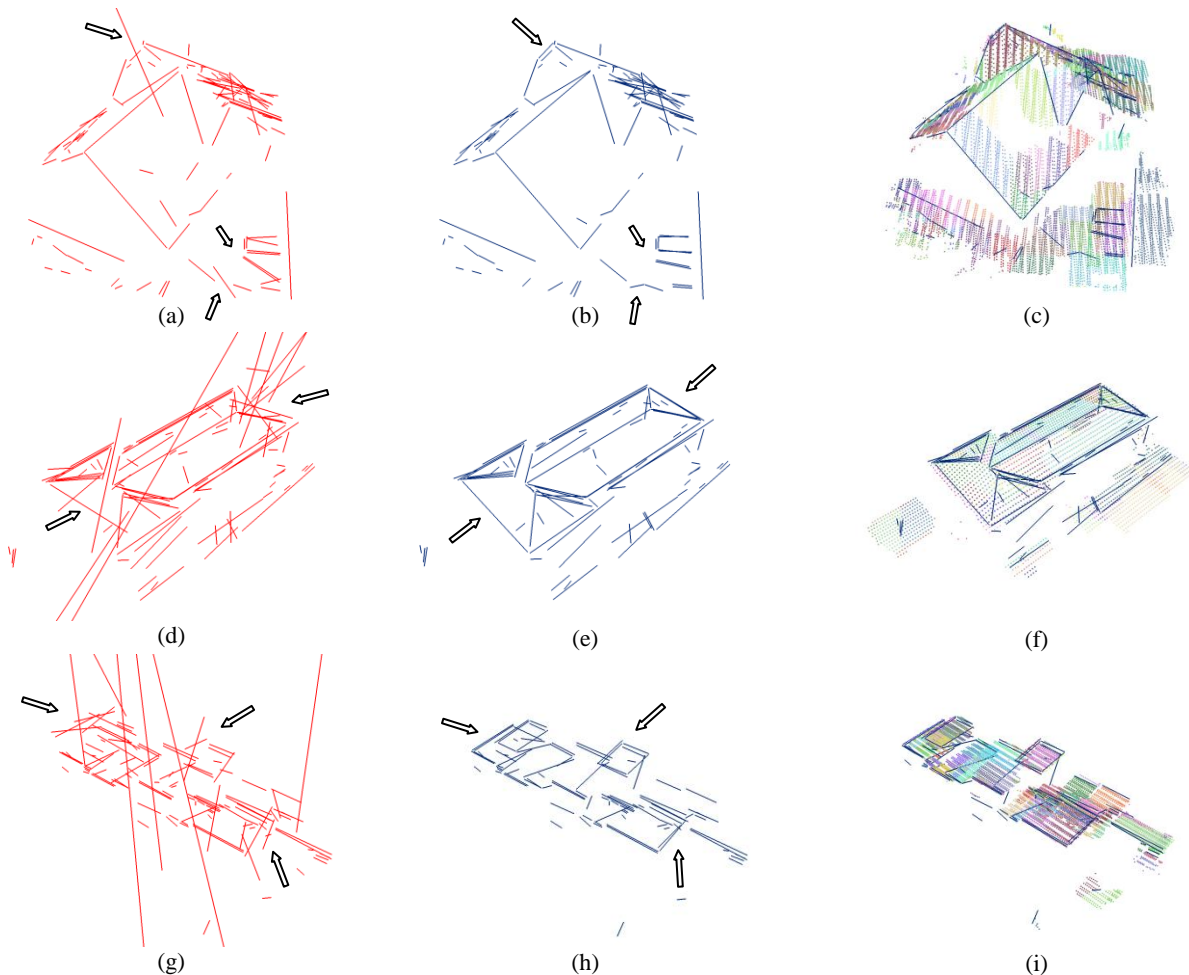

Fig. 8 3D line segments generated with the method of direct construction (a-d-g) and our approach (b-e-h). Block arrows point parts where some of the critical improvements are observed. The LIDAR point cloud overlaid with the lines reconstructed with our approach (c-f-i). Each color in the point cloud belongs to the automatically extracted 3D planes in the vicinity of each line.

Table 2. Comparison of the computed RMS distances of the Direct Construction method and the Proposed Approach

Patch ID	RMS Average Distance (m)					
	Direct Construction			Proposed Approach		
	Not-Aligned	Nearly-Aligned	Total	Not-Aligned	Nearly-Aligned	Total
1	0.152	1.041	0.495	0.152	0.357	0.204
2	0.173	4.451	2.240	0.173	0.196	0.179
3	0.194	6.278	3.768	0.194	0.459	0.275

RMS average distance between the reconstructed lines and the LIDAR planes. The results for each patch are given in Table 2. As expected, the method of direct construction produced reasonable RMS distances (≈ 2 pixels) for the line segments that are not aligned with the epipolar line. On the other hand, gross errors (> 1 m) are inevitable for the nearly-aligned cases, which also reduce the overall performance considerably. In contrast to the results of the direct construction, for each test patch, our approach led to massive RMS improvements after the reconstruction of the nearly-aligned line segments. Not surprisingly, in each case, this achievement reflects to the overall RMS performances as well.

5. CONCLUSIONS

In this paper, we proposed a new height estimation method for the line segments whose orientations in image space are found to be similar to the orientation of the epipolar line. The method manipulates the redundancy inherent in line pair-relations to generate artificial 3D point entities and utilize those entities during the estimation process to improve the height values of the reconstructed line segments. To test our approach, we selected three test patches over a built up area of the city of Vaihingen–Germany. Based on the results, the proposed approach produced highly promising reconstruction results for the line segments that are nearly-aligned with the epipolar line. Indeed, the final improvements are massive in terms of height accuracy; if we think that the results of the previous approaches that rely on just direct construction consistently result in gross height RMS errors (> 1 m). It is obvious that, the selected 3D point entities ($\mathbf{X}_i$) during the estimation process determine the final height quality of the 3D line estimated. In a worst-case scenario in which only a single 3D point entity is available, our method will not perform worse than the standard direct construction. Currently, we are extending the approach to deal with reconstruction drawbacks observed in image triplets that are acquired within a single strip.

ACKNOWLEDGEMENTS

REFERENCES

Bailard, C., Dissard, O., 2000, A stereo matching algorithm for urban digital elevation models. Photogrammetric Engineering and Remote Sensing, 66(9), pp. 1119-1128.

Cramer, M., Haala, N., 2009. DGPF Project: Evaluation of digital photogrammetric aerial based imaging systems – overview and results from the pilot centre. In: International Archives of the Photogrammetry, Remote Sensing and Spatial Information Sciences XXXVIII (1-4-7/W5), CD-ROM.

Förstner, W., Brunn, A., Heuel, S., 2000. Statistically Testing Uncertain Geometric Relations. In G. Sommer, N. Krüger, and Ch. Perwass, editors, Mustererkennung, pages 17-26. DAGM, Springer.

Förstner, W., 2005. Uncertainty and Projective Geometry, In: Bayro Corrochano, Eduardo (Hg.): Handbook of Geometric Computing. 2005, pp. 493-535.

Haala, N., 2009. Come Back of Digital Image Matching. Photogrammetric Week, Wichmann Verlag, Heidelberg, pp. 289-301.

Herbert, B., Vittorio, F., and Luc, V.G., 2005. Wide-baseline Stereo Matching with Line Segments, in: IEEE International Conference on Computer Vision and Pattern Recognition.

Heuel, S. and Förstner, W., 2001. Matching, reconstructing and grouping 3d lines from multiple views using uncertain projective geometry. In: CVPR '01, IEEE.

Heuel, S., 2001. Points, Lines and Planes and their Optimal Estimation . Proceedings of the DAGM 2001, pp 92-99.

Madsen, C. B., Christensen, H. I., 1995. Modeling and Testing the Stability of Edge Segments: Length and Orientation, SCIA pp. 1011-1019.

McGlone, C., Mikhail, E., and Bethel J., 2004. Manual of Photogrammetry. 5th Edition, Published by the American Society for Photogrammetry and Remote Sensing.

Ok, A. O., Wegner, J. D., Heipke, C., Rottensteiner, F., Soergel, U., and Toprak, V., 2010a. A New Straight Line Reconstruction Methodology From Multi-Spectral Stereo Aerial Images. Proceedings of Photogrammetric Computer Vision and Image Analysis Conference, Paris, IntArchPhRS Vol. 38(3A), pp. 25-30.

Ok, A. O., Wegner, J. D., Heipke, C., Rottensteiner, F., Soergel, U., and Toprak, V., 2010b. A Stereo Line Matching Technique For Aerial Images Based on A Pair-Wise Relation Approach, In: IntArchPhRS vol. XXXVIII-1/W17, Istanbul (on CD-ROM)

Rutzinger, M., Rottensteiner, F., Pfeifer, N., 2009. A comparison of evaluation techniques for building extraction from airborne laser scanning. IEEE Journal of Selected Topics in Applied Earth Observations and Remote Sensing, Vol. 2, No. 1, pp. 11-20.

Schmid, C. and Zisserman, A., 1997. Automatic Line Matching Across Views. In: Proceedings of CVPR, pp. 666–671.

Scholze, S., Moons, T., Ade, F., Van Gool, L., 2000. Exploiting Color for Edge Extraction and Line Segment Stereo Matching. In: IAPRS, 815–822.

Suveg, I., and Vosselman, G., 2004. Reconstruction of 3D Building Models from Aerial Images and Maps, ISPRS Journal of Photogrammetry and Remote Sensing, 58, pp. 202-224.

Zhang, C., Baltsavias, E. P., 2000. Edge matching and 3D road reconstruction using knowledge-based methods, Schriftenreihe der Fachrichtung Geodaesie, Darmstadt, Germany, 10, pp. 251-265.

Zhang, L., 2005. Automatic Digital Surface Model (DSM) Generation from Linear Array Images, PhD Thesis, Swiss Institute of Technology Zurich.